microPublication BIOLOGY

8/28/2025 - *Open Access*

The embryonic lethal mutation *zyg-10(b261)* is an allele of the *atx-2* gene and disrupts multiple aspects of early embryogenesis

Zachary G. Bell[1], Harold E. Smith[2], Kevin F. O'Connell[1§]

[1]Laboratory of Biochemistry and Genetics, National Institute of Diabetes and Digestive and Kidney Diseases, Bethesda, Maryland, United States

[2]Genomics Core, National Institute of Diabetes and Digestive and Kidney Diseases, Bethesda, Maryland, United States

[§]To whom correspondence should be addressed: kevino@nih.gov

Abstract

The *zyg-10(b261)* mutation was identified in one of the earliest screens for temperature-sensitive embryonic lethal mutations in *C. elegans*, but the cytological defects underlying the embryonic lethal phenotype, as well as the molecular identity of *zyg-10* had not been previously established. Here we show that *zyg-10(b261)* is an allele of the *atx-2* (ataxin-related) gene and that embryos produced by *atx-2(b261)* mothers exhibit a variety of defects including eggshell defects, cytokinesis failure, spindle mispositioning, and chromosome missegregation. We also show that the localization of separase, a regulator of egg-shell formation and mitosis, is defective in *atx-2(b261)* embryos.

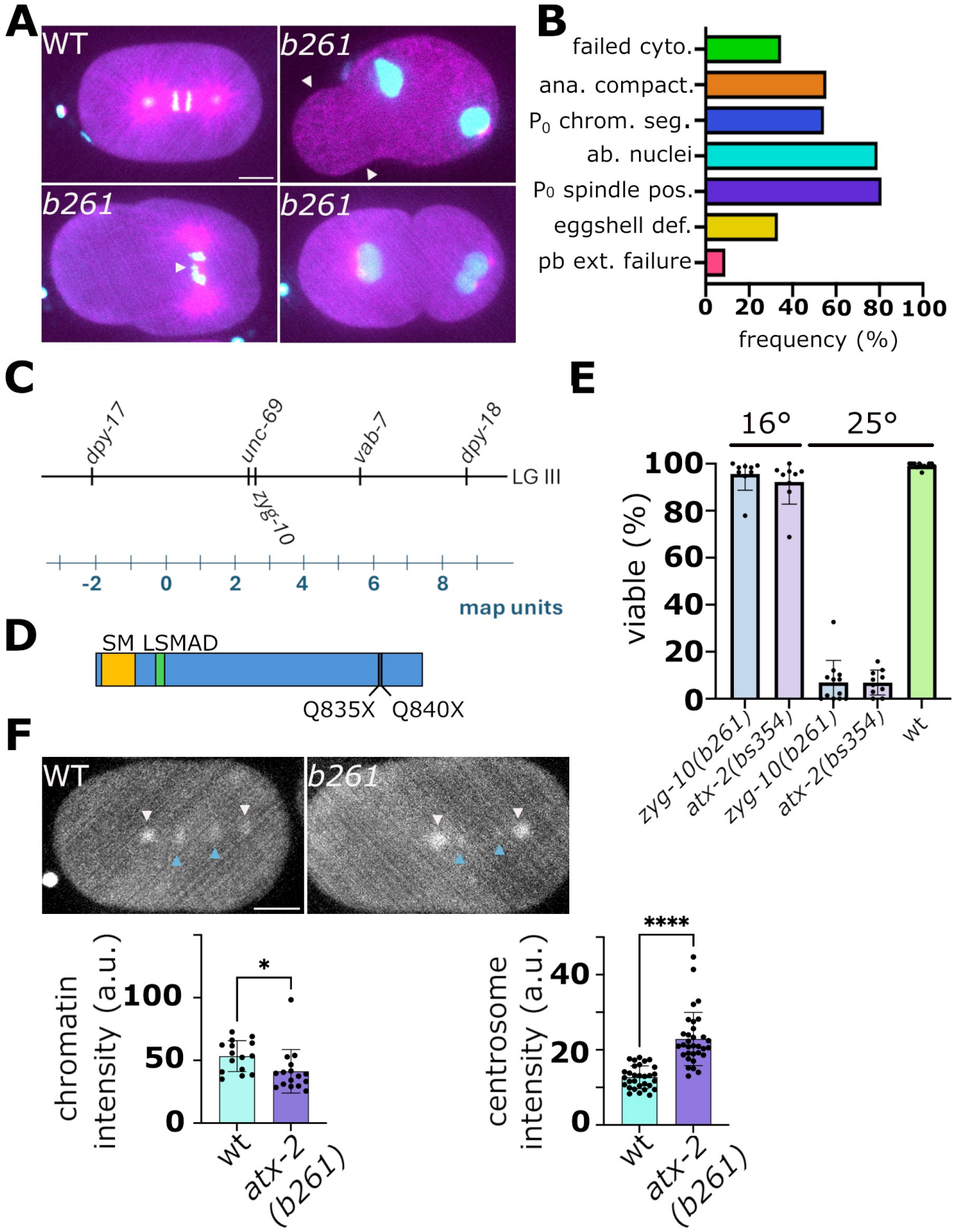

Figure 1. The *zyg-10(b261)* mutation is an allele of *atx-2*:

A. Select frames from recordings of wild-type and *zyg-10(b261)* embryos expressing GFP::histone (cyan) and mCherry::β-tubulin (magenta). At upper left is a wild-type embryo in anaphase. At upper right is a *zyg-10(b261)* embryo with a large cytoplasmic extension (arrowheads) which later resorbs, leading to a relatively normal-shaped embryo. This phenotype is likely due to an eggshell defect. At lower left is a mutant embryo with a mispositioned (transverse) spindle

and lagging chromosomes (arrowhead). At lower right is a two-cell mutant embryo with paired nuclei. Scale bar is 10 µm. **B.** Quantification of defects in *zyg-1(b261)* embryos (n=24). Defects listed are failed cytokinesis (failed cyto.), loss of anaphase compaction (ana compact.), a defect where individual chromosomes disperse during anaphase often leading to multiple nuclei, P_0 chromosome segregation defects (P_0 chrom. seg.), which includes failure to align all chromosomes on metaphase plate and/or lagging chromosomes, abnormal nuclei (ab. nuclei) which includes mishappen or paired nuclei, P_0 spindle mispositioning (P_0 spindle pos.), eggshell defects (eggshell def.), and polar body extrusion failure (pb ext. failure). By comparison, 14 wild-type embryos were scored with the only defect being one instance of a failed cytokinesis. No other abnormalities were detected. **C.** Map position of *zyg-10* as determined by three factor mapping. **D.** Schematic of the ATX-2 protein showing conserved SM and LSMAD domains and positions of truncations in *atx-2(ne4297*[Q835X]) and *atx-2(b261*[Q840X]) mutants. **E.** Embryonic viability of *zyg-10(b261)* and CRISPR allele *atx-2(bs354)* at 16° and 25°. Each datapoint represents the viability of offspring from a single hermaphrodite. Wild-type is included as a control. **F.** Representative images of wild-type and *atx-2(b261)* embryos expressing endogenously tagged SEP-1::GFP. Anaphase chromatin is marked with blue arrowheads and centrosomes with white arrowheads. The position of chromatin was followed by monitoring co-expressed mCherry::histone. Scale bar is 10 µm. The graphs shown below the images plot the integrated fluorescence intensity of SEP-1::GFP on chromosomes and centrosomes. Each data point represents the intensity from all chromatin in a single embryo or of individual centrosomes. * p< 0.05, **** p<0.0001. Statistical analysis of SEP-1::GFP intensity between wt and *zyg-10(b261)* was done with an unpaired t-test using the software Prism™ 10.

Description

The *zyg-10(b261)* mutation was identified in a pioneering screen for temperature-sensitive (ts) embryonic lethal mutations in 1980 (Wood *et al.* 1980), yet the underlying cause of the embryonic lethality as well as the molecular identity of *zyg-10* has remained a mystery. To address these issues, we sought to characterize the early divisions of *zyg-10(b261)* embryos expressing GFP::histone and mCherry::β-tubulin. We found that such mutants exhibit a variety of defects —most notably, a mispositioning of the P_0 spindle, which often assembles on a transverse axis (vs longitudinal in the wild type) at the posterior of the embryo (Figure 1A and B). This defect is consistent with earlier analysis which showed that *zyg-10(b261)* embryos undergo a skewed first cleavage resulting in a smaller than normal P_1 blastomere (Wood *et al.* 1980). However, we detected many other defects including misshapen or paired nuclei, chromosome segregation errors, and cytokinesis failure (Figure 1A and B). Thus, the *zyg-10(b261)* mutation affects many aspects of the early divisions.

We mapped *zyg-10* to position 2.6 between *unc-69* and *vab-7* on chromosome 3 (Figure 1C). Whole genome sequencing revealed that the *zyg-10(b261)* strain contained a nonsense mutation (Q840X) in the *atx-2* gene, which is located in the same genetic interval at position 2.51. Interestingly, the existing allele *atx-2(ne4297)* is also a premature stop (Q835X) mutation (Figure 1D) that confers a ts embryonic lethal phenotype marked by many of the same cytological defects as *zyg-10(b261)* (Gnazzo *et al.* 2016; Stubenvoll *et al.* 2016). We used CRISPR to recreate the Q840X mutation, designated *atx-2(bs354)*, and found that it produced a ts embryonic lethal phenotype that was similar in magnitude at both 16° and 25° to that of the *zyg-10(b261)* strain (Figure 1E). We conclude that *b261* is an allele of the *atx-2* gene and that the phenotypes specified in Figure 1E are due to disruption of ATX-2 function.

Interestingly, *atx-2* mutant embryos share many phenotypes with embryos lacking the mitotic regulator separase, including polar body extrusion failure, chromosome mis-segregation, eggshell defects, and cytokinesis failure (Siomos *et al.* 2001; Bembenek *et al.* 2007; Richie *et al.* 2011; Gnazzo *et al.* 2016; Stubenvoll *et al.* 2016). Thus, we decided to analyze the subcellular distribution of separase in *atx-2(b261)* embryos. Focusing on the portion of separase at the spindle, we found that SEP-1 levels were decreased moderately but significantly on chromatin, suggesting a possible cause for some of the chromosome segregation defects (Figure 1F). We also found that *atx-2(b261)* embryos have more separase at the spindle poles, possibly as a result of the enlarged centrosomes that are observed in the absence of ATX-2 (Stubenvoll *et al.* 2016). In summary we have established the molecular identity of *zyg-10* and provide evidence suggesting that mislocalization of separase may contribute so some of the defects observed in the absence of ATX-2.

Methods

For live imaging of embryos expressing GFP::histone and mCherry::β-tubulin, L4 stage worms were shifted to 25°C, 24 hours prior to imaging. Embryos were then dissected from gravid hermaphrodites in a 2 µl drop of egg buffer (188 mM NaCl, 48 mM KCl, 2 mM $CaCl_2$, 2 mM $MgCl_2$, 25 mM HEPES, pH 7.3) on a 12 mm circular coverslip. The coverslip was inverted and placed on a 3% agar/egg buffer pad that was cast in the well of a 0.25 mm thick ring-shaped spacer made of CultureWell™ Sheet Material (Grace Bio-Labs, Inc. Bend, OR) on a glass slide. A second glass slide was used to flatten the agar pad to the thickness of the spacer. Slides with embryos were transferred to a Thermo Plate heating/cooling stage (Tokai Hit USA Inc, Bala Cynwyd, PA) set at 25°C and were imaged using a spinning disk confocal microscope as previously described (Sankaralingam *et al.* 2024).

For live Imaging of SEP-1::GFP-expressing embryos, L4 stage worms were shifted to 24°C, 24 hours prior to imaging. Embryos were then dissected from gravid hermaphrodites in a 6 µl drop of meiosis medium (25 mM Hepes pH 7.4, 60% Leibowitz L-15 Media, 20% FBS, 500 µg/ml inulin) (Audhya et al. 2005) on a 12 mm circular coverslip. A glass slide containing a ring-shaped spacer as described above was then placed on top of the coverslip allowing the embryos to stay in suspension without pressure. Embryos were imaged and analyzed as above. All image analysis and processing was performed using ImageJ2 version 2.14.0/1.54f.

To determine the molecular identify of *zyg-10*, the *zyg-10(b261)* mutation was positioned on chromosome 3 via three-factor mapping as previously described (Brenner 1974). The *zyg-1(b261)* chromosome was placed over the *unc-69(e587) dpy-18(e364)* chromosome or the *dpy-17(e164) vab-7(e1562)* chromosome and hermaphrodites allowed to produce self-progeny. Recombinant (Dpy non-Unc/Unc non-Dpy or Dpy non-Vab/Vab non-Dpy respectively) progeny were then identified and picked to individual plates. For each recombinant, a line homozygous for the recombinant chromosome was established and the presence of the *zyg-10(b261)* mutation determined by screening for embryonic lethality at restrictive temperature.

For whole genome sequencing, worms were washed off a 100 mm high growth MYOB plate (3.5 mM Tris-HCl, 2 mM Tris-OH, 34 mM NaCl, 0.02 mM cholesterol , 20 g/L peptone, 30 g/L agar) in M9 buffer (22 mM KH_2PO_4, 22 mM Na_2HPO_4, 85 mM NaCl, 1 mM $MgSO_4$), spun for 3 minutes at 2095 x g and the excess M9 removed. The PureLink™ Genomic DNA Mini Kit (Catalog No. K1820-00, Thermo Fisher Scientific, Inc., Waltham, USA) was used to prepare genomic DNA following the “Mammalian Tissue and Mouse/Rat Tail Lysate” protocol. DNA concentration was measured using PicoGreen® and a TBS-380 Mini-Fluorometer (Turner BioSystems, Sunnyvale, USA). 100 µg of the genomic DNA was sheered using the Covaris S220 Focused-ultrasonicator and SonoLab 7 program (Covaris, LLC, Woburn, USA) to achieve an average fragment size of 300 base-pairs. A DNA library was prepared from the sheared DNA using the NEBNext® Ultra™ II DNA Library Prep Kit for Illumina®(Catalog No. E7103S, New England Biolabs, Ipswich, USA). The concentration of each library was again measured on the Mini-Fluorometer and quality assessed using the Agilent 2100 Bioanalyzer (Agilent Technologies, Inc, Savage, USA). The library was sequenced on the illumina HiSeq 3000 instrument (Illumina, Inc, San Diego, USA). Variant analysis was performed as described previously (SMITH, 2022) using a pipeline of BBMap 38.96 (BUSHNELL, 2022), SAMtools 1.16.1 (LI et al., 2009), FreeBayes 1.3.5 (GARRISON and MARTH, 2012), and ANNOVAR 2020-06-08 (WANG et al., 2010) with WormBase version WS277 as the reference genome. The sequencing data has been deposited at the Short Read Archive (https://www.ncbi.nlm.nih.gov/sra) under accession number SRR34981507.

CRISPR -Cas9 genome editing was performed as described previously (Sankaralingam *et al.* 2024)

Reagents

	Genotype	Source
DH261	*atx-2(b261[Q840X]) III*	CGC
OC1334	*atx-2(bs354[Q840X]) III*	OC
OC908	*bsSi30[pCW9: unc-119(+) pcdk-11.2::sfgfp::his-58::cdk-11.2 3' utr] II; bsIs20[pNP99: unc-119(+) tbb-1p::mCherry::tbb-2::tbb-2 3'-utr]; bsIs2 [pCK5.5: Ppie-1::gfp::spd-2]*	OC
OC1250	*bsSi30[pCW9: unc-119(+) pcdk-11.2::sfgfp::his-58::cdk-11.2 3' utr] II; atx-2(b261) III; bsIs20[pNP99: unc-119(+) tbb-1p::mCherry::tbb-2::tbb-2 3'-utr]*	OC
CB2233	*unc-69(e587) dpy-18(e364) III*	CGC
WM31	*dpy-17(e164) vab-7(e1562) III*	CGC
OC1329	*sep-1(it214[sep-1::gfp]) I, ltIs37 [pie-1p::mCherry::his-58 + unc-119(+)] IV*	OC
OC1331	*sep-1(it214[sep-1::gfp]) I; atx-2(b261) III; ltIs37 [pie-1p::mCherry::his-58 + unc-119(+)] IV*	OC

Reagents	**Source**

CultureWell™ Silicone Sheet Material	Grace Bio-Labs Cat # CWS-S-0.25
12 mm circular cover glass	Fisher Scientific Cat# 12541001
PureLink™ Genomic DNA Mini Kit	ThermoFisher Scientific Cat # K1820-00
NEBNext® Ultra™ II DNA Library Prep Kit for Illumina®	New England Biolabs, Cat # E7103S

CRISPR	**Sequence**
b261 crRNA	5'-UCAACAGUAUAUGGUGAUGC-3'
b261 Repair Template	5'-GCAGCAGCAGCAGCAACACATTCAACAGTATATGGTGATGtAGGGCCCGC ATCAAATGCATCCGCAGATCCCTAATTACTATCAGC-3'

Acknowledgements: Some strains were provided by the CGC, which is funded by NIH Office of Research Infrastructure Programs (P40 OD010440).

References

Audhya A, Hyndman F, McLeod IX, Maddox AS, Yates JR 3rd, Desai A, Oegema K. 2005. A complex containing the Sm protein CAR-1 and the RNA helicase CGH-1 is required for embryonic cytokinesis in Caenorhabditis elegans. J Cell Biol 171(2): 267-79. PubMed ID: 16247027

Bembenek JN, Richie CT, Squirrell JM, Campbell JM, Eliceiri KW, Poteryaev D, et al., White JG. 2007. Cortical granule exocytosis in C. elegans is regulated by cell cycle components including separase. Development 134(21): 3837-48. PubMed ID: 17913784

Brenner S. 1974. The genetics of Caenorhabditis elegans. Genetics 77(1): 71-94. PubMed ID: 4366476

Bushnell, B., 2022 BBmap. SourceForge. Available from: https://sourceforge.net/projects/bbmap.

Garrison, E. and Marth, G., 2012 Haplotype-based variant detection from short-read sequencing. *arXiv* 1207.3907. 10.48550/arXiv.1207.3907

Gnazzo MM, Uhlemann EE, Villarreal AR, Shirayama M, Dominguez EG, Skop AR. 2016. The RNA-binding protein ATX-2 regulates cytokinesis through PAR-5 and ZEN-4. Mol Biol Cell 27(20): 3052-3064. PubMed ID: 27559134

Li H, Handsaker B, Wysoker A, Fennell T, Ruan J, Homer N, et al., 1000 Genome Project Data Processing Subgroup. 2009. The Sequence Alignment/Map format and SAMtools. Bioinformatics 25(16): 2078-9. PubMed ID: 19505943

Richie CT, Bembenek JN, Chestnut B, Furuta T, Schumacher JM, Wallenfang M, Golden A. 2011. Protein phosphatase 5 is a negative regulator of separase function during cortical granule exocytosis in C. elegans. J Cell Sci 124(Pt 17): 2903-13. PubMed ID: 21878498

Sankaralingam P, Wang S, Liu Y, Oegema KF, O'Connell KF. 2024. The kinase ZYG-1 phosphorylates the cartwheel protein SAS-5 to drive centriole assembly in C. elegans. EMBO Rep 25(6): 2698-2721. PubMed ID: 38744971

Siomos MF, Badrinath A, Pasierbek P, Livingstone D, White J, Glotzer M, Nasmyth K. 2001. Separase is required for chromosome segregation during meiosis I in Caenorhabditis elegans. Curr Biol 11(23): 1825-35. PubMed ID: 11728305

Smith HE. 2022. Mutation Mapping and Identification by Whole-Genome Sequencing. Methods Mol Biol 2468: 257-269. PubMed ID: 35320569

Stubenvoll MD, Medley JC, Irwin M, Song MH. 2016. ATX-2, the C. elegans Ortholog of Human Ataxin-2, Regulates Centrosome Size and Microtubule Dynamics. PLoS Genet 12(9): e1006370. PubMed ID: 27689799

Wang K, Li M, Hakonarson H. 2010. ANNOVAR: functional annotation of genetic variants from high-throughput sequencing data. Nucleic Acids Res 38(16): e164. PubMed ID: 20601685

Wood WB, Hecht R, Carr S, Vanderslice R, Wolf N, Hirsh D. 1980. Parental effects and phenotypic characterization of mutations that affect early development in Caenorhabditis elegans. Dev Biol 74(2): 446-69. PubMed ID: 7371984

8/28/2025 - *Open Access*

Funding: This research was supported by the Intramural Research Program of the National Institute of Diabetes and Digestive and Kidney Diseases (NIDDK) within the National Institutes of Health (NIH). The contributions of the NIH author(s) are considered Works of the United States Government. The findings and conclusions presented in this paper are those of the author(s) and do not necessarily reflect the views of the NIH or the U.S. Department of Health and Human Services.

Author Contributions: Zachary G. Bell: investigation, writing - review editing, methodology. Harold E. Smith: investigation, data curation, methodology, writing - review editing. Kevin F. O'Connell: formal analysis, funding acquisition, project administration, writing - original draft, writing - review editing.

Reviewed By: Anonymous

Nomenclature Validated By: Anonymous

WormBase Paper ID: WBPaper00068539

History: Received June 23, 2025 **Revision Received** August 14, 2025 **Accepted** August 27, 2025 **Published Online** August 28, 2025 **Indexed** September 11, 2025

Citation: Bell ZG, Smith HE, O'Connell KF. 2025. The embryonic lethal mutation *zyg-10(b261)* is an allele of the *atx-2* gene and disrupts multiple aspects of early embryogenesis. microPublication Biology. 10.17912/micropub.biology.001714